EUROPEAN ORGANIZATION FOR NUCLEAR RESEARCH (CERN)

CERN-EP-2022-098
2022/06/13

CMS-HIN-21-009

Observation of τ lepton pair production in ultraperipheral lead-lead collisions at $\sqrt{s_{\mathrm{NN}}} = 5.02\,\mathrm{TeV}$

The CMS Collaboration

Abstract

We present an observation of photon-photon production of τ lepton pairs in ultraperipheral lead-lead collisions. The measurement is based on a data sample with an integrated luminosity of 404 $\mu\mathrm{b}^{-1}$ collected by the CMS experiment at a nucleon-nucleon center-of-mass energy of 5.02 TeV. The $\gamma\gamma \to \tau^+\tau^-$ process is observed for $\tau^+\tau^-$ events with a muon and three charged hadrons in the final state. The measured fiducial cross section is $\sigma(\gamma\gamma \to \tau^+\tau^-) = 4.8 \pm 0.6\,(\mathrm{stat}) \pm 0.5\,(\mathrm{syst})\,\mu\mathrm{b}$, in agreement with leading-order QED predictions. Using $\sigma(\gamma\gamma \to \tau^+\tau^-)$, we estimate a model-dependent value of the anomalous magnetic moment of the τ lepton of $a_\tau = 0.001^{+0.055}_{-0.089}$ at a 68% confidence level.

Submitted to Physical Review Letters

Ultraperipheral collisions (UPCs) of nuclei, where the impact parameter is larger than the sum of the nuclear radii, provide an extremely clean environment to study various photon-induced processes [1]. For the case of lead-lead (PbPb) UPCs, the production cross section for two-photon fusion processes is enhanced by a factor of about Z^4 (where $Z = 82$ is the Pb charge number), relative to proton-proton collisions. The possibility of observing photon-induced τ lepton production in UPC events at a heavy ion collider was considered well before the LHC era [2]. Recently, theoretical studies [3, 4] have proposed that kinematic properties of τ lepton pairs produced in heavy ion UPCs at the LHC can be used to constrain the electromagnetic couplings of the τ lepton. These constraints allow for fundamental tests of quantum electrodynamics (QED) and for probing beyond the standard model (BSM) physics.

A contributing factor in the coupling of leptons (ℓ) to photons (γ) is the anomalous magnetic moment $a_\ell = (g-2)_\ell/2$, with the gyromagnetic ratio g being the proportionality constant that relates the magnetic moment to the spin of the lepton. With 12 significant digits, the electron anomalous magnetic moment a_e is among the most precisely measured quantities [5], and differs from the standard model (SM) expectation by either -2.4 or $+1.6$ standard deviations [5, 6], depending on the input value of the fine structure constant, α_QED. The value of a_μ has been measured to 9 significant figures [7]. It shows a tension of $+4.2$ standard deviations with respect to SM predictions [8], although a calculation with a modified hadronic contribution [9] reduces the discrepancy between data and theory by a factor of more than 2, albeit with an uncertainty that is about 20% larger. While the predicted a_τ value is $0.00117721\,(5)$ [10, 11], its currently best measured value is $-0.018\,(17)$, at a 68% confidence level, from the DELPHI Collaboration [12]. This primarily results from the short τ lepton lifetime, which is of the order of 10^{-13} s, such that τ leptons cannot be stored long enough to measure their a_τ-dependent precession in a magnetic field. A more precise a_τ determination will facilitate tighter constraints on BSM physics searches [13, 14], and might be particularly important considering the tensions observed in semi-leptonic decays of b hadrons [15–33]. This motivates employing novel experimental approaches at the LHC.

In this Letter, we present an observation of τ lepton pairs in ultraperipheral PbPb collisions, $\gamma\gamma \to \tau^+\tau^-$, in events that may contain excitations of the outgoing Pb ions. With this measurement, the CMS Collaboration begins its systematic exploitation of heavy ion beams at the LHC as a powerful probe of a_τ. The analysis is based on a data sample with an integrated luminosity of $404\,\mu\mathrm{b}^{-1}$ collected by the CMS experiment in 2015 at a nucleon-nucleon center-of-mass energy of $\sqrt{s_\mathrm{NN}} = 5.02\,\mathrm{TeV}$. One τ lepton is reconstructed through its decay to one muon and two neutrinos, while the other is reconstructed through its "3 pronged" decay into charged hadrons plus a neutrino [34]. This choice of final state offers a clean experimental signature, with the muon used for online selection and the hadronically decaying τ candidate providing discrimination against dimuon photoproduction and an unambiguous reconstruction of τ lepton decay. The reconstruction of the τ leptons is performed over a fiducial phase space, defined by the transverse momentum (p_T) and pseudorapidity (η) of each particle, in order to maximize the signal purity and efficiency. Tabulated results are provided in the HEPData record for this analysis [35].

The CMS apparatus [36] is a multipurpose, nearly hermetic detector, designed to trigger on [37, 38] and identify electrons, muons, photons, and hadrons [39–41]. A global reconstruction "particle-flow" algorithm [42] combines the information provided by the all-silicon inner tracker and by the crystal electromagnetic, and the brass and scintillator hadron calorimeters, operating inside a 3.8 T superconducting solenoid, with data from gas-ionization muon detectors embedded in the flux-return yoke outside the solenoid, to build τ leptons, jets, and missing p_T [43–45]. Forward hadron (HF) calorimeters [46], made of steel and quartz-fibers, extend the

η coverage ($3.0 < |\eta| < 5.2$) provided by the barrel and endcap detectors. The HF calorimeters are segmented to form 0.175×0.175 "towers" ($\Delta\eta \times \Delta\phi$, with ϕ being the azimuthal angle). Events are filtered using a two-tiered trigger system. The first level, composed of custom hardware processors, uses information from the calorimeters and muon detectors [37]. The second level, known as the high-level trigger [38], consists of a farm of processors running a version of the full event reconstruction software.

The UPCs producing two final-state τ leptons are uniquely characterized by low track multiplicity and the presence of very forward (i.e., high $|\eta|$) lead ions that are either scattered or dissociated in a direction so close to the beam as to be undetectable. Therefore, we select high-purity UPC events [47] by requiring in real time the presence of a single muon with no explicit p_{T} threshold requirement and at least one pixel detector track, as well as by setting an upper limit on the event activity in the HF [37]. To further suppress background processes, such as hadronic PbPb collisions, it is required offline that the leading-energy tower measured by the HF is below 4 GeV.

Furthermore, the signal phase space region is constrained offline by selecting events with one muon and exactly three additional tracks. For the muon from the "τ_{μ}" candidate, a selection is applied requiring $|\eta| < 2.4$ and that the muon be"soft" [40]. The requirement on the p_{T} varies depending on the muon $|\eta|$, and is $p_{\mathrm{T}} > 3.5\,\mathrm{GeV}$ for $|\eta| < 1.2$ and $p_{\mathrm{T}} > 2.5\,\mathrm{GeV}$ for $|\eta| > 1.2$, following the muon detector system reconstruction acceptance. The three tracks that form the "$\tau_{3\mathrm{prong}}$" candidate [43] are assumed to be pions and are required to be within the tracker acceptance ($|\eta| < 2.5$), have a common vertex within 2.5 mm of the primary vertex along the direction of the two beams, and be identified as charged hadrons by the particle-flow algorithm. The transverse momentum of the leading (i.e. highest p_{T}) and two subleading pions must be greater than 0.5 and 0.3 GeV, respectively. The selected tracks are also required to pass the "high-purity" requirements of Ref. [41]. The $\tau_{3\mathrm{prong}}$ candidate is then required to be of opposite charge relative to the selected τ_{μ}, and to have $p_{\mathrm{T}}^{\mathrm{vis}} > 2\,\mathrm{GeV}$, where $p_{\mathrm{T}}^{\mathrm{vis}}$ is the vector sum p_{T} of the three charged pions (the "visible" decay products of $\tau_{3\mathrm{prong}}$). Additionally, the invariant mass of the three pion candidates m_{τ}^{vis} is required to be between 0.2 and 1.5 GeV. The event selection defining the fiducial phase space in this paper is summarized in Table 1. These selections identify 91 $\gamma\gamma \to \tau^{+}\tau^{-}$ candidate events.

Table 1: Summary of the event selection, which defines the fiducial phase space region for the $\sigma(\gamma\gamma \to \tau^{+}\tau^{-})$ measurement.

Muon selection	$p_{\mathrm{T}} > 3.5\,\mathrm{GeV}$ for $\lvert\eta\rvert < 1.2$
	$p_{\mathrm{T}} > 2.5\,\mathrm{GeV}$ for $1.2 < \lvert\eta\rvert < 2.4$
Pion selection	$p_{\mathrm{T}} > 0.5\,\mathrm{GeV}$ for the leading
	$p_{\mathrm{T}} > 0.3\,\mathrm{GeV}$ for the (sub-)subleading
	$\lvert\eta\rvert < 2.5$
$\tau_{3\mathrm{prong}}$ selection	$p_{\mathrm{T}}^{\mathrm{vis}} > 2\,\mathrm{GeV}$ and $0.2 < m_{\tau}^{\mathrm{vis}} < 1.5\,\mathrm{GeV}$

Backgrounds arise from heavy quark photoproduction, UPC photon-photon interactions producing scalar mesons, and photon-pomeron interactions producing vector and pseudoscalar mesons that can generate events with muons and charged hadrons. Dedicated samples of events from $\gamma\gamma \to \tau^{+}\tau^{-}$ [3], $\gamma\gamma \to \mathrm{c\bar{c}}$, and $\gamma\gamma \to \mathrm{b\bar{b}}$ processes are generated with MADGRAPH5_aMC@NLO (v2.6.5) [48], where PYTHIA8 (v2.1.2) [49] is used for the hadronization and decay, and GEANT4 [50] is used to model the detector effects, including resolution, tracking,

and trigger efficiencies. Distributions of the muons and charged pions in simulated events are corrected using comparisons between the simulation and data, outside the signal region, as a function of the muon or track p_T and η. For muons, we use a "tag-and-probe" method with $J/\psi \to \mu^+\mu^-$ events [40], and for charged hadrons, we use the ratio of reconstructed D^0 meson decays to final states with four charged hadrons divided by those with two daughters. The simulated background processes produce a large number of tracks and hence sparsely populate the signal-dominated phase space region. They are only used to partly validate the expected $\gamma\gamma \to c\bar{c}$ and $\gamma\gamma \to b\bar{b}$ contributions to the background estimation as described in the following paragraph.

To properly estimate the background, we use a technique based on control samples in data, referred to as the "ABCD method". Three phase space regions ("categories") are used to derive the background in the fourth region, from which the signal is extracted. The four categories, which have been found to be uncorrelated in data, are defined according to the number of charged tracks per event (n_{ch}) and the energy of the tower in HF. The low-n_{ch} categories (B and D) are defined by $n_{ch} = 3$, whereas the high-n_{ch} categories (A and C) must have $5 \leq n_{ch} \leq 8$ to avoid signal contamination while being similar to the signal region. The low-HF (C and D) and high-HF (A and B) categories are defined by energies below and above 4 GeV, respectively. Consequently, category D is the signal region (low-n_{ch} and low-HF category), and the background estimation is $B_i C_i / A_i$, where each of the categories is evaluated for the different kinematic bins, as indicated by the i subscript. Based on the simulated signal events, we find that the event selection described above removes all signal events from the control regions (A–C). The kinematic distributions showing the $\gamma\gamma \to \tau^+\tau^-$ signal process, scaled to match the QED prediction of Ref. [3], as well as the background model based on control samples in data, are shown in Fig. 1. Good agreement is observed between the measured distributions and the sum of the signal simulation and background estimation.

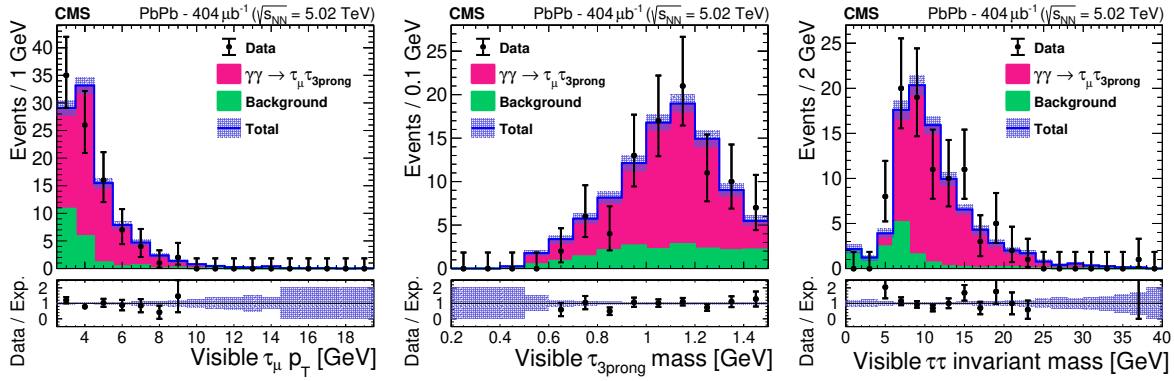

Figure 1: Left: Transverse momentum of the muon originating from the τ_μ candidate. Middle: Invariant mass of the three pions forming the τ_{3prong} candidate. Right: $\tau^+\tau^-$ invariant mass. In all plots, the signal component (magenta histogram) is stacked on top of the background component (green histogram), considering their initial normalizations, as described in the text. The sum of signal and background is displayed by a blue line and the shaded area shows the statistical uncertainty. The data are represented with black points and the uncertainty is statistical only. The lower panels show the ratios of data to the signal-plus-background prediction, and the shaded bands represent the statistical uncertainty in the prefit expectation.

A binned maximum likelihood fit of signal and background components is used for the signal extraction. The fit is performed on the binned distribution of the difference in azimuthal opening angle between the τ_μ and τ_{3prong} candidates, $\Delta\phi(\tau_\mu, \tau_{3prong})$, exploiting the fact that the two signal τ leptons are produced azimuthally back-to-back in UPCs [1, 51]. The signal dis-

tribution is derived from simulation, while that of the background is obtained from the ABCD method described above, including its normalization as a constant parameter in the fit. The prefit number of signal events is scaled to match the QED prediction of Ref. [3]. Systematic uncertainties may affect both the normalization and the shape of the $\Delta\phi(\tau_\mu, \tau_{3\text{prong}})$ distributions. These uncertainties, in addition to the bin-by-bin variations of the signal and background templates, are represented by nuisance parameters in the fit. Rate-changing nuisance parameters are represented as log-normal probability distribution functions, while shape-changing ones are represented with Gaussian probability distribution functions. The negative of the log likelihood is minimized by varying the nuisance parameters according to their uncertainties and by scaling the signal by a multiplicative factor r.

Uncertainties arising from the HF energy threshold are evaluated by varying the HF energy by 10% [52]. The effect on the measured cross section due to this variation is dominated by the resulting variation in the background shape from the ABCD procedure, and is found to be 0.9%. An additional systematic uncertainty coming from the background shape and yield estimation is considered by reevaluating the background using the ABCD procedure, changing the high n_{ch} parameter to individual values of 5, 6, 7, and 8, as opposed to the range 5–8. The maximum variation with respect to the central value comes from the determination with $n_{\text{ch}} = 5$, resulting in a 0.2% variation of the fiducial cross section measurement.

The uncertainty in the muon efficiency, including the trigger response, identification and tracking efficiency, has an impact of 6.7%. The integrated luminosity is measured with the methods described in Refs. [53, 54], and has an uncertainty of 5%, which affects the yield from the QED simulation to which the signal is normalized. The uncertainty in the pion tracking efficiency results in an uncertainty of 3.6%. The simulated signal distribution has a finite number of events, resulting in a 3% uncertainty due to bin-by-bin statistical fluctuations, and a 1.1% weighted binomial uncertainty on the efficiency. The uncertainty in the τ lepton branching fraction measurements is 0.6% [34]. The uncertainties described above are summarized in Table 2 and the total uncertainty, obtained by adding them in quadrature while taking into account their correlation, is found to be 9.7%.

Table 2: Postfit contributions to the systematic uncertainty of the $\sigma(\gamma\gamma \to \tau^+\tau^-)$ measurement, in percent. The last row gives the sum in quadrature of all components while taking into account their correlation.

Source	Uncertainty (%)
Muon efficiency	6.7
Integrated luminosity measurement	5
Pion efficiency	3.6
Simulation sample size (bin-by-bin)	3.0
Simulation sample size (efficiency)	1.1
HF scale effect on background shape	0.9
τ lepton branching fraction	0.6
Effect of n_{ch} on background shape	0.2
Total	9.7

The best fit value of the signal strength multiplicative factor is $r = 0.99^{+0.16}_{-0.14}$ with $N_{\text{sig}} = 77 \pm 12$ signal events in the integral of the postfit signal component. The fit result is shown in Fig. 2, along with the data, and signal and background templates. The observed (expected) signal significance, computed using the asymptotic approximation [55], is found to be 14.2 (14.5) stan-

dard deviations. These values indicate a clear observation of the $\gamma\gamma \to \tau^+\tau^-$ process.

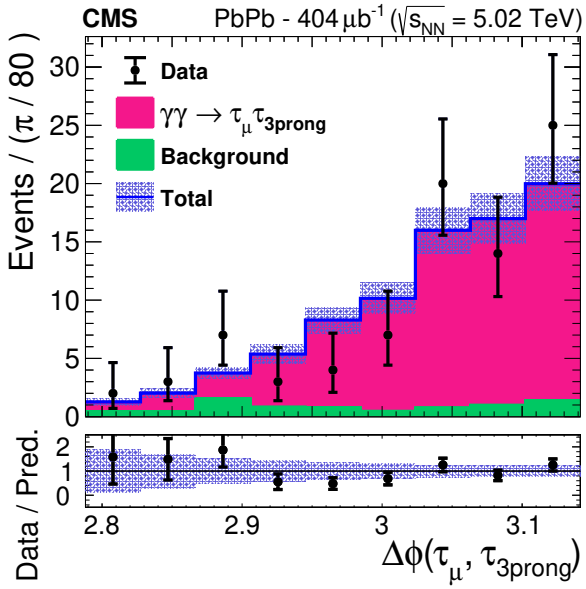

Figure 2: Difference in azimuthal opening angle between the τ_μ and τ_{3prong} candidates. The data are represented by the points with the vertical bars showing the statistical uncertainties. The signal (background) contribution is given by the magenta (green) histogram, after the application of the fit procedure. The total is displayed by a blue line and the shaded area shows the combined statistical and systematic uncertainties. The lower panel shows the ratio of data to the signal plus background prediction, and the shaded band represents the total uncertainty in the postfit prediction.

The cross section is measured in the fiducial volume of the CMS detector, following the kinematic requirements previously described and summarized in Table 1. The formula used is $\sigma(\gamma\gamma \to \tau^+\tau^-) = N_{sig}/(2\epsilon\,\mathcal{L}_{int}\,\mathcal{B}_{\tau_\mu}\,\mathcal{B}_{\tau_{3prong}})$, where N_{sig} is the number of signal events estimated by the fit process, ϵ is the total signal efficiency, $\mathcal{L}_{int}$ is the total integrated luminosity, and $\mathcal{B}_{\tau_\mu}$ and $\mathcal{B}_{\tau_{3prong}}$ are the branching fractions for the two τ lepton decay modes. The factor of two accounts for the two potential τ lepton decay combinations yielding the same final state. The integrated luminosity corresponds to $\mathcal{L}_{int} = 404 \pm 20\,\mu b^{-1}$. The branching fractions are are $\mathcal{B}_{\tau_\mu} = (17.39 \pm 0.04)\%$ and $\mathcal{B}_{\tau_{3prong}} = (14.55 \pm 0.06)\%$ [34]. The efficiency is the convolution of the pion and muon reconstruction, the trigger, and the analysis selection efficiencies, and is evaluated using simulated signal events. The efficiency is calculated as the number of reconstructed events passing the analysis selection criteria divided by the number of generated events inside the fiducial phase space region, and is found to be $\epsilon = (78.5 \pm 0.8)\%$.

Combining all of the above, the fiducial cross section is found to be $\sigma(\gamma\gamma \to \tau^+\tau^-) = 4.8 \pm 0.6\,(stat) \pm 0.5\,(syst)\,\mu b$. The result, summarized in Fig. 3, is compared to leading-order QED predictions [3, 4]. The analytical calculation from Ref. [4] results in a cross section which is 20% higher than that found in Ref. [3]. This is explained in Ref. [4] as mainly stemming from the different requirements applied in the modeling of single-photon fluxes. In both cases, although further theory advancements are needed for a proper uncertainty evaluation, a conservative uncertainty of 10% is considered following the approach from Ref. [47] given the similarity of final states and phase-space volumes.

Recent calculations have evaluated the impact of BSM processes on the $\gamma\gamma \to \tau^+\tau^-$ cross section. The BSM coupling variations in a_τ can change the expected cross section and alter

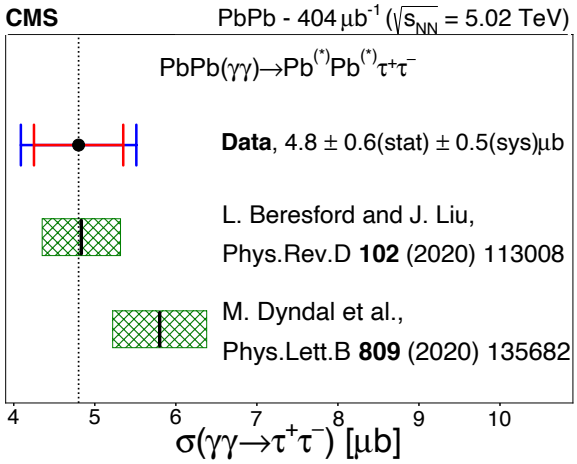

Figure 3: The cross section, $\sigma(\gamma\gamma \to \tau^+\tau^-)$, measured in a fiducial phase space region at $\sqrt{s_{\mathrm{NN}}} = 5.02\,\mathrm{TeV}$. The theoretical predictions [3, 4] are computed with leading-order accuracy in QED and are represented by the vertical solid lines that can be compared with the vertical dotted line representing this measurement. The outer blue (inner red) error bars surrounding the data point indicate the total (statistical) uncertainties, whereas the green hatched bands correspond to the uncertainty in the theoretical predictions as described in the main text. The potential electromagnetic excitation of the outgoing Pb ions is denoted by $(^*)$.

the τ lepton p_{T} spectrum [3, 4]. We assume the correction factor of Ref. [3] to extrapolate the fiducial cross section measurement (Table 1) to the full phase space region, after taking into account an extra factor of $1/\sqrt{4\pi}$ for the electron charge in Heaviside-Lorentz units. We then use variations of the total $\sigma(\gamma\gamma \to \tau^+\tau^-)$ as a function of a_τ to extract a model-dependent value of a_τ at the LHC. The measured value is $a_\tau = 0.001^{+0.055}_{-0.089}$ at a 68% confidence level, which is consistent with the current best measurement [12]. The ATLAS Collaboration has also recently reported a measurement of $\gamma\gamma \to \tau^+\tau^-$ using a larger PbPb luminosity from 2018 [56]. With respect to this measurement, we cover a larger phase space with muon $p_{\mathrm{T}} > 2.5\,\mathrm{GeV}$ while Ref. [56] uses $p_{\mathrm{T}} > 4\,\mathrm{GeV}$, and we make no restrictions on neutron emission. We also make use of a complementary approach of extracting a_τ from $\sigma(\gamma\gamma \to \tau^+\tau^-)$, while Ref. [56] extracts a_τ from a shape analysis of the τ_μ p_{T}. Because of the larger fiducial phase space region comprised by this measurement, the attained precision in the studied final state is comparable to that in Ref. [56].

In summary, an observation of τ lepton pair production in ultraperipheral nucleus-nucleus collisions is reported. Events with a final state of one muon and three charged hadrons assumed to be pions are reconstructed from a lead-lead data sample with an integrated luminosity of $404\,\mu\mathrm{b}^{-1}$ collected by the CMS experiment at $\sqrt{s_{\mathrm{NN}}} = 5.02\,\mathrm{TeV}$ in 2015. The statistical significance of the signal relative to the background-only expectation is above five standard deviations. The cross section for the $\gamma\gamma \to \tau^+\tau^-$ process, within a fiducial phase space region, is $\sigma(\gamma\gamma \to \tau^+\tau^-) = 4.8 \pm 0.6\,(\mathrm{stat}) \pm 0.5\,(\mathrm{syst})\,\mu\mathrm{b}$, in agreement with leading-order quantum electrodynamics predictions. Using the measured cross section and its corresponding uncertainties, we estimate a model-dependent value of the anomalous magnetic moment of the τ lepton of $a_\tau = 0.001^{+0.055}_{-0.089}$ at a 68% confidence level. This measurement provides a novel experimental probe of the τ anomalous magnetic moment using heavy ion collisions at the LHC.

References

[1] A. J. Baltz, "The physics of ultraperipheral collisions at the LHC", *Phys. Rept.* **458** (2008) doi:10.1016/j.physrep.2007.12.001, arXiv:0706.3356.

[2] F. del Aguila, F. Cornet, and J. I. Illana, "The possibility of using a large heavy ion collider for measuring the electromagnetic properties of the τ lepton", *Phys. Lett. B* **271** (1991) 256, doi:10.1016/0370-2693(91)91309-J.

[3] L. Beresford and J. Liu, "New physics and τ $g-2$ using LHC heavy ion collisions", *Phys. Rev. D* **102** (2020) 113008, doi:10.1103/PhysRevD.102.113008, arXiv:1908.05180.

[4] M. Dyndal, M. Klusek-Gawenda, M. Schott, and A. Szczurek, "Anomalous electromagnetic moments of τ lepton in $\gamma\gamma \to \tau^+\tau^-$ reaction in PbPb collisions at the LHC", *Phys. Lett. B* **809** (2020) 135682, doi:10.1016/j.physletb.2020.135682, arXiv:2002.05503.

[5] R. H. Parker et al., "Measurement of the fine-structure constant as a test of the standard model", *Science* **360** (2018) 191, doi:10.1126/science.aap7706, arXiv:1812.04130.

[6] L. Morel, Z. Yao, P. Cladé, and S. Guellati-Khélifa, "Determination of the fine-structure constant with an accuracy of 81 parts per trillion", *Nature* **588** (2020) 61, doi:10.1038/s41586-020-2964-7.

[7] Muon $g-2$ Collaboration, "Measurement of the positive muon anomalous magnetic moment to 0.46 ppm", *Phys. Rev. Lett.* **126** (2021) 141801, doi:10.1103/PhysRevLett.126.141801, arXiv:2104.03281.

[8] T. Aoyama et al., "The anomalous magnetic moment of the muon in the standard model", *Phys. Rept.* **887** (2020) 1, doi:10.1016/j.physrep.2020.07.006, arXiv:2006.04822.

[9] S. Borsanyi et al., "Leading hadronic contribution to the muon magnetic moment from lattice QCD", *Nature* **593** (2021) 51, doi:10.1038/s41586-021-03418-1, arXiv:2002.12347.

[10] M. Passera, "Precise mass-dependent QED contributions to leptonic $g-2$ at order α^2 and α^3", *Phys. Rev. D* **75** (2007) 013002, doi:10.1103/PhysRevD.75.013002, arXiv:hep-ph/0606174.

[11] S. Eidelman and M. Passera, "Theory of the τ lepton anomalous magnetic moment", *Mod. Phys. Lett. A* **22** (2007) 159, doi:10.1142/S0217732307022694, arXiv:hep-ph/0701260.

[12] DELPHI Collaboration, "Study of τ pair production in photon-photon collisions at LEP and limits on the anomalous electromagnetic moments of the τ lepton", *Eur. Phys. J. C* **35** (2004) 159, doi:10.1140/epjc/s2004-01852-y, arXiv:hep-ex/0406010.

[13] A. Crivellin, M. Hoferichter, and J. M. Roney, "Towards testing the magnetic moment of the τ at one part per million", 2021. arXiv:2111.10378.

[14] A. Crivellin and M. Hoferichter, "Consequences of chirally enhanced explanations of $(g-2)_\mu$ for $h \to \mu\mu$ and $Z \to \mu\mu$", *JHEP* **07** (2021) 135, doi:10.1007/JHEP07(2021)135, arXiv:2104.03202.

[15] BaBar Collaboration, "Evidence for an excess of $\overline{B} \to D^* \tau^- \overline{\nu}_\tau$ decays", *Phys. Rev. Lett.* **109** (2012) 101802, doi:10.1103/PhysRevLett.109.101802, arXiv:1205.5442.

[16] BaBar Collaboration, "Measurement of an excess of $\overline{B} \to D^* \tau^- \overline{\nu}_\tau$ decays and implications for charged Higgs bosons", *Phys. Rev. D* **88** (2013) 072012, doi:10.1103/PhysRevD.88.072012, arXiv:1303.0571.

[17] Belle Collaboration, "Measurement of the branching ratio of $\overline{B} \to D^* \tau^- \overline{\nu}_\tau$ relative to $\overline{B} \to D^* \ell^- \overline{\nu}_\ell$ decays with hadronic tagging at Belle", *Phys. Rev. D* **92** (2015) 072014, doi:10.1103/PhysRevD.92.072014, arXiv:1507.03233.

[18] Belle Collaboration, "Measurement of the branching ratio of $\overline{B}^0 \to D^{*+} \tau^- \overline{\nu}_\tau$ relative to $\overline{B}^0 \to D^{*+} \ell^- \overline{\nu}_\ell$ decays with a semileptonic tagging method", *Phys. Rev. D* **94** (2016) 072007, doi:10.1103/PhysRevD.94.072007, arXiv:1607.07923.

[19] Belle Collaboration, "Measurement of the τ lepton polarization and $R(D^*)$ in the decay $\overline{B} \to D^* \tau^- \overline{\nu}_\tau$", *Phys. Rev. Lett.* **118** (2017) 211801, doi:10.1103/PhysRevLett.118.211801, arXiv:1612.00529.

[20] Belle Collaboration, "Measurement of the τ lepton polarization and $R(D^*)$ in the decay $\overline{B} \to D^* \tau^- \overline{\nu}_\tau$ with one-prong hadronic τ decays at Belle", *Phys. Rev. D* **97** (2018) 012004, doi:10.1103/PhysRevD.97.012004, arXiv:1709.00129.

[21] Belle Collaboration, "Measurement of $\mathcal{R}(D)$ and $\mathcal{R}(D^*)$ with a semileptonic tagging method", *Phys. Rev. Lett.* **124** (2020) 161803, doi:10.1103/PhysRevLett.124.161803, arXiv:1910.05864.

[22] LHCb Collaboration, "Measurement of the ratio of branching fractions $\mathcal{B}(\overline{B}^0 \to D^{*+} \tau^- \overline{\nu}_\tau)/\mathcal{B}(\overline{B}^0 \to D^{*+} \mu^- \overline{\nu}_\mu)$", *Phys. Rev. Lett.* **115** (2015) 111803, doi:10.1103/PhysRevLett.115.111803, arXiv:1506.08614. [Erratum: doi:10.1103/PhysRevLett.115.159901].

[23] LHCb Collaboration, "Measurement of the ratio of the $B^0 \to D^{*-} \tau^+ \nu_\tau$ and $B^0 \to D^{*-} \mu^+ \nu_\mu$ branching fractions using three-prong τ-lepton decays", *Phys. Rev. Lett.* **120** (2018) 171802, doi:10.1103/PhysRevLett.120.171802, arXiv:1708.08856.

[24] LHCb Collaboration, "Measurement of the ratio of branching fractions $\mathcal{B}(B_c^+ \to J/\psi \tau^+ \nu_\tau)/\mathcal{B}(B_c^+ \to J/\psi \mu^+ + \nu_\mu)$", *Phys. Rev. Lett.* **120** (2018) 121801, doi:10.1103/PhysRevLett.120.121801, arXiv:1711.05623.

[25] Belle Collaboration, "Lepton-flavor-dependent angular analysis of $B \to K^* \ell^+ \ell^-$", *Phys. Rev. Lett.* **118** (2017) 111801, doi:10.1103/PhysRevLett.118.111801, arXiv:1612.05014.

[26] LHCb Collaboration, "Measurement of form-factor-independent observables in the decay $B^0 \to K^{*0} \mu^+ \mu^-$", *Phys. Rev. Lett.* **111** (2013) 191801, doi:10.1103/PhysRevLett.111.191801, arXiv:1308.1707.

[27] LHCb Collaboration, "Differential branching fractions and isospin asymmetries of $B \to K^* \mu^+ \mu^-$ decays", *JHEP* **06** (2014) 133, doi:10.1007/JHEP06(2014)133, arXiv:1403.8044.

[28] LHCb Collaboration, "Test of lepton universality using $B^+ \to K^+\ell^+\ell^-$ decays", *Phys. Rev. Lett.* **113** (2014) 151601, doi:10.1103/PhysRevLett.113.151601, arXiv:1406.6482.

[29] LHCb Collaboration, "Angular analysis of the $B^0 \to K^{*0}\mu^+\mu^-$ decay using $3\,\text{fb}^{-1}$ of integrated luminosity", *JHEP* **02** (2016) 104, doi:10.1007/JHEP02(2016)104, arXiv:1512.04442.

[30] LHCb Collaboration, "Angular analysis and differential branching fraction of the decay $B_s^0 \to \phi\mu^+\mu^-$", *JHEP* **09** (2015) 179, doi:10.1007/JHEP09(2015)179, arXiv:1506.08777.

[31] LHCb Collaboration, "Test of lepton universality with $B^0 \to K^{*0}\ell^+\ell^-$ decays", *JHEP* **08** (2017) 055, doi:10.1007/JHEP08(2017)055, arXiv:1705.05802.

[32] LHCb Collaboration, "Search for lepton-universality violation in $B^+ \to K^+\ell^+\ell^-$ decays", *Phys. Rev. Lett.* **122** (2019) 191801, doi:10.1103/PhysRevLett.122.191801, arXiv:1903.09252.

[33] LHCb Collaboration, "Test of lepton universality in beauty quark decays", *Nature Phys.* **18** (2022) 277, doi:10.1038/s41567-021-01478-8, arXiv:2103.11769.

[34] Particle Data Group, "Review of Particle Physics", *PTEP* **2020** (2020) 083C01, doi:10.1093/ptep/ptaa104.

[35] CMS, 2022. doi:10.17182/hepdata.129600.

[36] CMS Collaboration, "The CMS experiment at the CERN LHC", *JINST* **3** (2008) S08004, doi:10.1088/1748-0221/3/08/S08004.

[37] CMS Collaboration, "Performance of the CMS level-1 trigger in proton-proton collisions at $\sqrt{s} = 13\,\text{TeV}$", *JINST* **15** (2020) P10017, doi:10.1088/1748-0221/15/10/P10017, arXiv:2006.10165.

[38] CMS Collaboration, "The CMS trigger system", *JINST* **12** (2017) P01020, doi:10.1088/1748-0221/12/01/P01020, arXiv:1609.02366.

[39] CMS Collaboration, "Electron and photon reconstruction and identification with the CMS experiment at the CERN LHC", *JINST* **16** (2021) P05014, doi:10.1088/1748-0221/16/05/P05014, arXiv:2012.06888.

[40] CMS Collaboration, "Performance of the CMS muon detector and muon reconstruction with proton-proton collisions at $\sqrt{s} = 13\,\text{TeV}$", *JINST* **13** (2018) P06015, doi:10.1088/1748-0221/13/06/P06015, arXiv:1804.04528.

[41] CMS Collaboration, "Description and performance of track and primary-vertex reconstruction with the CMS tracker", *JINST* **9** (2014) P10009, doi:10.1088/1748-0221/9/10/P10009, arXiv:1405.6569.

[42] CMS Collaboration, "Particle-flow reconstruction and global event description with the CMS detector", *JINST* **12** (2017) P10003, doi:10.1088/1748-0221/12/10/P10003, arXiv:1706.04965.

[43] CMS Collaboration, "Performance of reconstruction and identification of τ leptons decaying to hadrons and ν_τ in pp collisions at $\sqrt{s} = 13\,\text{TeV}$", *JINST* **13** (2018) P10005, doi:10.1088/1748-0221/13/10/P10005, arXiv:1809.02816.

[44] CMS Collaboration, "Jet energy scale and resolution in the CMS experiment in pp collisions at 8 TeV", *JINST* **12** (2017) P02014, doi:10.1088/1748-0221/12/02/P02014, arXiv:1607.03663.

[45] CMS Collaboration, "Performance of missing transverse momentum reconstruction in proton-proton collisions at $\sqrt{s} = 13$ TeV using the CMS detector", *JINST* **14** (2019) P07004, doi:10.1088/1748-0221/14/07/P07004, arXiv:1903.06078.

[46] CMS Collaboration, "Calibration of the CMS hadron calorimeters using proton-proton collision data at $\sqrt{s} = 13$ TeV", *JINST* **15** (2020) P05002, doi:10.1088/1748-0221/15/05/P05002, arXiv:1910.00079.

[47] CMS Collaboration, "Evidence for light-by-light scattering and searches for axion-like particles in ultraperipheral PbPb collisions at $\sqrt{s_{\mathrm{NN}}} = 5.02$ TeV", *Phys. Lett. B* **797** (2019) 134826, doi:10.1016/j.physletb.2019.134826, arXiv:1810.04602.

[48] J. Alwall et al., "The automated computation of tree-level and next-to-leading order differential cross sections, and their matching to parton shower simulations", *JHEP* **07** (2014) 079, doi:10.1007/JHEP07(2014)079, arXiv:1405.0301.

[49] T. Sjöstrand et al., "An introduction to PYTHIA 8.2", *Comput. Phys. Commun.* **191** (2015) 159, doi:10.1016/j.cpc.2015.01.024, arXiv:1410.3012.

[50] GEANT4 Collaboration, "GEANT4—a simulation toolkit", *Nucl. Instrum. Meth. A* **506** (2003) 250, doi:10.1016/S0168-9002(03)01368-8.

[51] CMS Collaboration, "Observation of forward neutron multiplicity dependence of dimuon acoplanarity in ultraperipheral PbPb Collisions at $\sqrt{s_{\mathrm{NN}}} = 5.02 TeV$", *Phys. Rev. Lett.* **127** (2021) 122001, doi:10.1103/PhysRevLett.127.122001, arXiv:2011.05239.

[52] CMS Collaboration, "Measurement of exclusive Υ photoproduction from protons in pPb collisions at $\sqrt{s_{\mathrm{NN}}} = 5.02$ TeV", *Eur. Phys. J. C* **79** (2019) 277, doi:10.1140/epjc/s10052-019-6774-8, arXiv:1809.11080.

[53] CMS Collaboration, "Precision luminosity measurement in proton-proton collisions at $\sqrt{s} = 13$ TeV in 2015 and 2016 at CMS", *Eur. Phys. J. C* **81** (2021) 800, doi:10.1140/epjc/s10052-021-09538-2, arXiv:2104.01927.

[54] CMS Collaboration, "CMS luminosity measurement using nucleus-nucleus collisions at $\sqrt{s_{\mathrm{NN}}} = 5.02$ TeV in 2018", CMS Physics Analysis Summary CMS-PAS-LUM-18-001, 2022.

[55] G. Cowan, K. Cranmer, E. Gross, and O. Vitells, "Asymptotic formulae for likelihood-based tests of new physics", *Eur. Phys. J. C* **71** (2011) 1554, doi:10.1140/epjc/s10052-011-1554-0, arXiv:1007.1727. [Erratum: doi:10.1140/epjc/s10052-013-2501-z].

[56] ATLAS Collaboration, "Observation of the $\gamma\gamma \to \tau\tau$ process in PbPb collisions and constraints on the τ lepton anomalous magnetic moment with the ATLAS detector", 2022. arXiv:2204.13478. Submitted to *Phys. Rev. Lett.*